Kassab *et al. J Wireless Com Network* (2022) 2022:77
https://doi.org/10.1186/s13638-022-02151-1

EURASIP Journal on Wireless Communications and Networking

RESEARCH Open Access

Superposition of rectangular power pulses and CP-OFDM signal for SWIPT

Hussein Kassab*, François Rottenberg, Thomas Feuillen, Charles Wiame and Jérôme Louveaux

*Correspondence:
hussein.kassab@uclouvain.be

Institute of Information and Communication Technologies, Electronics and Applied Mathematics, 1348 Louvain la Neuve, Belgium

Abstract

Simultaneous wireless information and power transfer (SWIPT) has recently attracted researchers and may help to satisfy future technology demands. SWIPT allows wireless power transfer (WPT) and wireless information transfer (WIT) to coexist based on shared resources. Recent studies have shown that, due to the nonlinearity of the rectifiers, high-PAPR (peak to average power ratio) waveforms provide better performance in terms of energy harvesting, making the design of power signals essential. In addition, these power signals should consume the smallest amount of resources for the WIT.
In this paper, a new waveform design is proposed where the information and power signals are superposed using the same frequency and time resources. The power signal is composed of a high peak modulated rectangular wave sent during the cyclic prefix of the orthogonal frequency-division multiplexing (CP-OFDM) system, which is discarded at the information receiver, such that it does not interfere with the OFDM data symbol. Although the pulse is restricted to be within the cyclic prefix, there might be a small amount of interference caused by channel dispersion. Simulations and measurements show that a good choice of signal parameters can minimize interference on the information symbols and simultaneously provide good performance in terms of energy harvesting.

Keywords: SWIPT, WPT, WIT, Energy harvesting, Waveform design, CP-OFDM, Nonlinear rectifier model

1 Introduction

1.1 Background and motivations

Internet of things (IoT) electronic devices such as battery-free sensors, passive radio frequency identification (RFID), and machine-to-machine (M2M) systems are expected to be extensively deployed in the near future. Beside their need for wireless information transfer (WIT), it is envisioned that these devices could harvest energy from the nearby electromagnetic sources or from dedicated power heads in order to extend their battery lifetime. The harvesting of energy is done using a harvester known as "rectenna" which is composed of an antenna concatenated with a rectifier. This dual demand of information and power attracted the research community to investigate simultaneous wireless information and power transfer (SWIPT), which consists of transferring both energy and information wirelessly using the same radio frequency resources [1, 2]. One possible

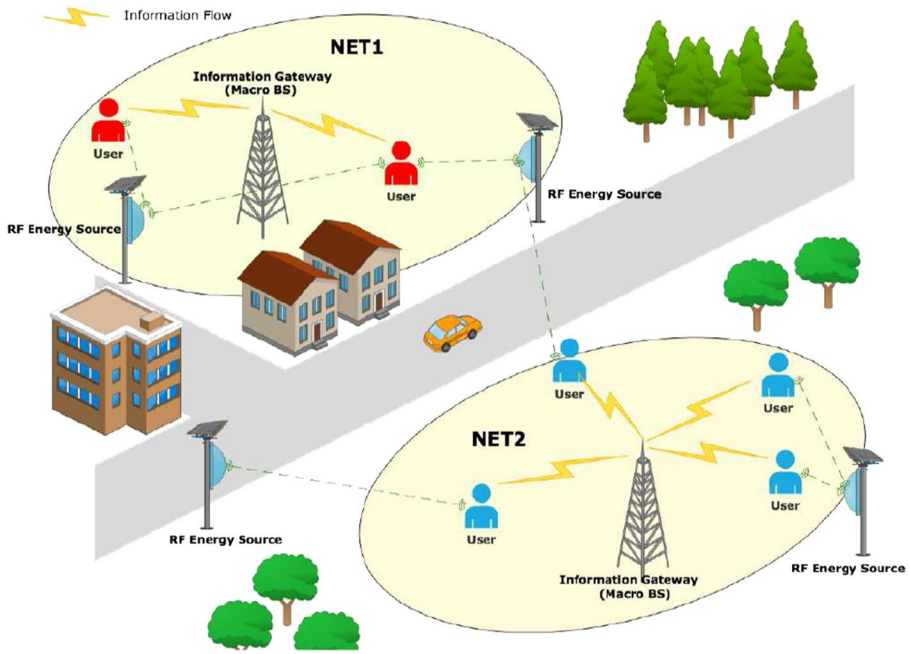

Fig. 1 Illustration of a SWIPT network structure showing a possible scenario of coexistence between WIT and WPT

scenario of coexistence between WIT and wireless power transfer (WPT) systems is illustrated in Fig. 1.

SWIPT was first introduced by [3] where the fundamental trade-off between energy and information was addressed showing that the rate-energy (R-E) region is a non-increasing concave function. A substantial interest in SWIPT has been observed in the communication literature, focusing on different aspects: wireless powered communication [4–6], MIMO broadcasting [7–9], interference channel [10–12], relaying [13–15], broadband system [16–18]. Another aspect is the receiver architecture [19] which can be either separate receiver [7], power-splitting [19], time switching [17], antenna switching [20], or as suggested by [21] to jointly extract information and harvest power without consuming energy in the process of collecting decoded data. Recently, an end-to-end machine learning approach was studied in [22] to jointly optimize the transmitter and the receiver using neural network (NN)-based auto-encoders. Also, a closed-loop practical SWIPT prototype with adaptive waveform optimization based on channel state information (CSI) acquisition and different receiver architectures is implemented in the works of [23, 24]. The work in [25, 26] provides a comprehensive survey of state-of-the-art SWIPT techniques. Besides, the works in [27, 28] provide interesting overviews of potential applications and promising future research paths for SWIPT.

In the early literature, no specific waveform design for the power signal was considered since the RF energy harvester was based on a linear model that depends only on the received power [25]. Hence, the power signal was usually set as a single tone. However, when the nonlinearity of the rectifier is considered, it has been noticed that the output DC current not only depends on the circuit parameters but also on the input waveform design [2, 29]. In addition, it has been shown in [30, 31] that high-PAPR waveforms

provide better performance in terms of energy harvesting. Accordingly, waveform design became an important factor that should be considered while maximizing the energy harvested to make the best out of an available RF spectrum for the same transmitter power.

In the case of SWIPT, the WPT waveform design has to be taken into consideration jointly with everything that is related to the information transfer. Several methods were proposed to have an optimized waveform design for both power and information signals (i.e., SWIPT waveform design). This waveform design can be based either on a combined waveform (i.e., one common signal for both WPT and WIT) or on separate waveforms (i.e., two signals that are clearly distinct but share the same resources). One approach for combining waveforms was addressed in [32], where a multisine waveform is used for energy transfer with distinct levels of PAPR acting as information transfer, enabling a low-energy combined receiver. However, this has a very limited data rate. Other methods using combined waveforms are studied in the works of [33–35]. The idea is to utilize one common OFDM signal for both WPT and WIT. The information receiver stays the same while the cyclic prefix is not discarded and instead used for harvesting energy. However, in many practical communication systems, the received power is limited and hence the resulting harvested energy might not be sufficient for most applications (and might even sometimes not be sufficient to activate the rectifier). Regarding the separate waveform approach, one way to implement it is to divide the resources in a time-frequency grid as proposed in [36]. Another way, proposed in [37], is to superpose a multisine power signal with a CP-OFDM information signal and use a cancellation scheme at the receiver. This has the advantage of sharing the resources simultaneously, but the method might suffer from saturation of the ADC (Analog to Digital Converter) when the power signal is of much higher level than the information signal.

One common obstacle that SWIPT systems face is the large discrepancy between the power sensitivity for energy harvesting and information decoding. The received power for standard communication systems can be in the range of -60 dBm. On the other hand, WPT operates in a much higher power range, around -10 dBm and it requires higher power levels to trigger and turn on the rectifier at the receiver [38]. For this reason, it is a necessity to have the power head located only few meters away from the receiver while base stations can be located farther away from the receiver. In view of these opposite requirements when designing waveform for SWIPT, it is more convenient to consider separate waveforms for WPT and WIT. It is also more practical from network structure point of view to consider different transmitter nodes for WPT and WIT where each one operates with a different power and range. In addition, since there is a huge gap of power between both systems, the practical design should make sure that the high power levels of the WPT system does not cause interference, nor ADC saturation, nor any other negative effect on the information decoding chain.

In conclusion, to the best of our knowledge, none of the works in the literature were able to fulfil all of the following objectives at the same time:

- O.1 Establishing SWIPT by sharing the same resources among both WPT and WIT systems.
- O.2 Designing the system to match simultaneously the very different power requirements for WPT and WIT.

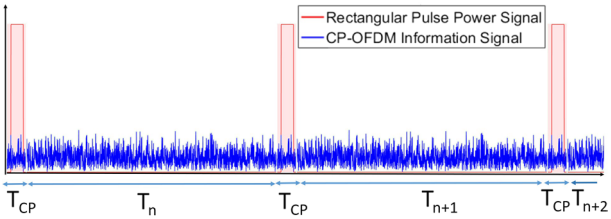

Fig. 2 Proposed waveform by superposing WPT and WIT signals in a synchronized fashion

O.3 Avoiding interference, ADC saturation, and other possible degradation of WIT performance.

O.4 Considering high-PAPR power signal to increase WPT performance taking into account the nonlinear model of the rectifier.

In this work, we consider a practical system design that takes into account all of the above aspects at the same time. The first basic idea of this design was first presented in our work in [39]. It assumes that WIT signal uses a standard cyclic-prefix orthogonal frequency-division multiplexing (CP-OFDM) while the WPT signal is a modulated rectangular wave signal that is sent during the cyclic prefix and is silent during the useful part of the OFDM symbol (see Fig. 2). It also assumes that WIT and WPT transmitters are physically separated and require time synchronization to minimize interference. However, even though the rectangular pulse is restricted to be within the cyclic prefix duration, there might still be a small amount of interference generated by the leakage of the WPT signal into the useful OFDM data caused by channel dispersion. So, our work in [39]:

1 Proposes a new waveform design for SWIPT by superposing WIT and WPT in synchronized fashion.
2 Provides interference evaluation of WPT onto WIT with its corresponding simulation results.
3 Provides measurement results for the performance of the proposed waveform in terms of energy harvesting only and not for information decoding. These measurements show that, for a fixed average power, the narrower is the width of the proposed rectangular waveform, the better is the energy harvesting performance.

1.2 Novelty and contributions

In this publication, we go further in the waveform design as well as in the analysis of the WPT and WIT coexistence by expanding our work in [39] by:

1 Proving that the proposed waveform is optimal by providing the necessary logical and mathematical reasoning to justify the choice of the rectangular shape.
2 Investigating the influence of the proposed power signal onto the complete information decoding chain of the receiver. In particular, the following points are important:

- Studying the effect of the power pulse signal on the frame synchronization.

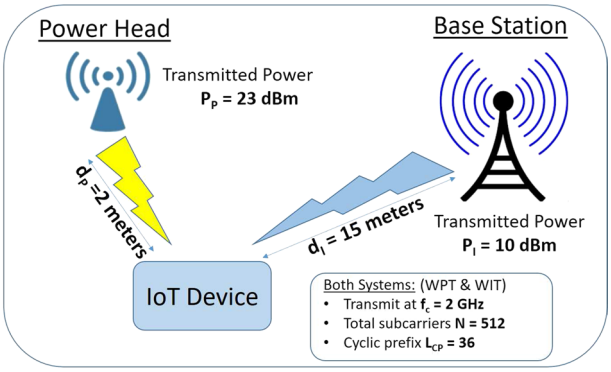

Fig. 3 Practical example of an heterogeneous network used with a power head, a base station, and an IoT receiver located 15 m away from the base-station and 2 m only from the power head. For example in an indoor scenario, the power head is in the same room as the IoT receiver while the base-station can be in a different room

- Investigating possible ADC saturation.

3 Conducting real measurements to validate the simulation results and study in reality the impact of WPT on the complete decoding chain of WIT. Specifically, we analyzed the influence on WIT performance when the power gap between both systems is very large.

The paper is organized as follows: first, the system model including the wireless network structure and information signal model are introduced in Sect. 2. The power waveform design is studied in Sect. 3 including the choice of waveform shape, waveform parameters, and waveform design subject to regulations and limitations. The influence of the power signal on the information decoding chain including the components, signal processing operations, and influenced data (with interference analysis and simulations) is discussed in Sect. 4. Measurements setup and results are presented in Sect. 5. Finally, the paper is concluded in Sect. 6.

Notations: Scalars are noted as x, vectors are bold as $\mathbf{x}$. * is the convolution operation.

2 System model

2.1 Wireless network structure

There are more than one setup to illustrate SWIPT architecture where its concept is to allow both systems WPT and WIT coexist within the same network. Fig. 1 is one example of a possible scenario where SWIPT can be achieved. Recall that we consider separate transmitters for each system because the operating range for WPT is much higher than that of WIT creating a huge power gap between both systems. Therefore, the network that we consider in our work is a simple heterogeneous network that is illustrated in Fig. 3. It consists of a combination of the following:

- Power transmitter (or power head)
- The information transmitter (or base station)
- The battery-free IoT device that contains:

- A chain for information decoding
- A chain for energy harvesting (i.e., a rectifier)
- Both chains can either have different antennas or share the same antenna with either time switching (TS) or power splitting (PS) strategies. There is no preference for a certain receiver architecture and it is not studied in this work.

In order to have a sufficient amount of harvested energy, the distance between the power head and the IoT receiver should be reasonably small. So it is more appropriate to consider a network setup where the IoT receiver is only few meters away from the power transmitter. An example of such network setup is an indoor environment or a highly dense urban outdoor network.

As mentioned earlier, the proposed design considers that the WIT system utilizes standard CP-OFDM as a multi-carrier scheme for data transmission between the base station and the IoT device. Also, the WPT signal consists of a high peak pulse that is transmitted during the cyclic prefix duration. Both systems, WIT and WPT, are assumed to be precisely synchronized in time using a backhaul or any other relevant strategy. Considering that our design is SWIPT, WPT and WIT share the same frequency band $\mathcal{B}$.

2.2 Information signal model and parameters

The standard CP-OFDM is used for wireless information transmission between the base station and the IoT device. The discrete-time representation of the transmitted baseband OFDM signal defined on ($0 \leq m \leq N + L_{\text{cp}}$) can be written as:

$$x_I[m] = \sum_{n=0}^{N-1} s_n e^{J\frac{2\pi(n-L_{\text{cp}})}{N}m}, \tag{1}$$

where s_n is the symbol transmitted on the nth subcarrier, L_{cp} is the cyclic prefix length (in number of samples), and N represents the number of subcarriers. The useful OFDM data duration is denoted as $T = NT_{\text{s}}$, where T_{s} is the sampling period of the system. The time duration of the cyclic prefix is denoted as $T_{\text{cp}} = L_{\text{cp}}T_{\text{s}}$. The subcarrier spacing is defined as $\Delta_f = \frac{1}{T}$. On the other hand, the power signal will be studied in detail in the next section.

3 Power waveform design

In this section, we provide an overall reasoning and mathematical justification behind the proposed design of the power signal.

3.1 Design constraints and objectives

As already mentioned above, the goal of this design is to superpose the power and the information signals in such a way that the high power WPT signal interferes as little as possible onto the information signal. To do so, and considering that the samples within the cyclic prefix can be discarded at the receiver, the power signal is sent as a pulse during the cyclic prefix duration only, repeated periodically at every cyclic prefix.

Looking back on the objectives of the waveform design listed in the introduction section, we can say that objectives 0.1 and 0.2 are already satisfied in this design. However,

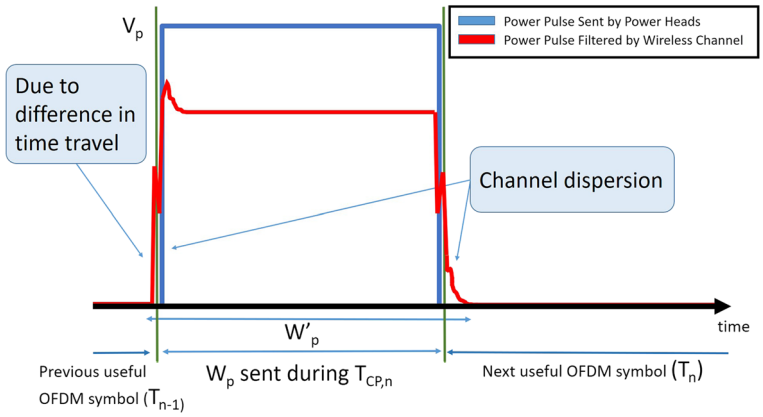

Fig. 4 Effect of Wireless channel dispersion of the power signal onto the previous and successive useful OFDM symbol

objectives 0.3 and 0.4 leave a room for pulse optimization such as its shape, duration, and other aspects. According to objective 0.3, the design should avoid degradation of WIT performance by reducing the risk of interference. Particularly, the wireless channel dispersion from the power head to the IoT device causes the pulse signal to spread longer in time (as illustrated in Fig. 4) which may lead to interference on the next OFDM symbols. Therefore, the pulse should end the furthest away possible from the end of the cyclic prefix to allow for some margin. In general, the pulse should have the smallest possible duration (in time) in order to avoid interference on the useful OFDM symbol. As for objective 0.4, the power signal should maximize the energy harvested at the receiver taking into account the nonlinear model of the rectifier. According to [30], high-PAPR signals usually increase WPT performance. The measurements in [39] confirm this claim that WPT is better with high-peak signals. Besides, from the transmitter point of view, it is important to note that the high-peak power signals increase the efficiency of the power amplifier (PA). On the other hand, the regulations impose limitation on both the total power transmitted by the signal and its PAPR, where the PAPR Υ is defined as the ratio between the peak power P_{P} and the average power P_{av} i.e., $\Upsilon = \frac{P_{\mathrm{P}}}{P_{\mathrm{av}}}$. The regulations state that the peak power should not exceed 20 dB above the average power [40]. Hence, the three important elements that need to be considered for SWIPT pulse optimization based on the above discussion are as follows:

1 The pulse should be designed to maximize the energy harvested according to the rectifier model.
2 The pulse should respect the transmit power and peak power constraints.
3 If possible, the pulse should have a short time duration to minimize the interference on the information part.

Considering the above points, it can be shown that the best possible waveform satisfying these conditions is the rectangular-shaped pulse (in equivalent baseband) where a limited average transmitted power P_{av} is utilized with a maximum possible peak during the smallest duration. The mathematical justification is provided in the next subsection.

3.2 Optimization of the power signal

Let us consider the design of a modulated power pulse $w_{\mathrm{p}}(t)$ with a band limited baseband that is sent during the CP duration, of length T_{cp}. The power pulse is repeated every CP-OFDM symbol, i.e., every $T + T_{\mathrm{cp}}$, where T is the useful OFDM data duration. The transmitted power signal in passband can be written as:

$$w(t) = \Re\left[w_{\mathrm{P}}(t)e^{J\omega_{\mathrm{c}}t}\right] = \frac{1}{2}w_{\mathrm{P}}(t)e^{J\omega_{\mathrm{c}}t} + \frac{1}{2}w_{\mathrm{P}}(t)^{*}e^{-J\omega_{\mathrm{c}}t}, \tag{2}$$

where ω_{c} is the carrier frequency. We assume that the bandwidth of the power pulse is very small compared to the carrier frequency ($\mathcal{B} << \omega_{\mathrm{c}}$). We also assume that the channel is ideal so that the received signal is exactly $w(t)$.

Considering the nonlinear model of the rectifier in [2], which is based on a simple single-diode rectifier (diode and RC circuit), the harvested current i_{out} can be approximated by a Taylor series as

$$i_{\mathrm{out}} = \sum_{i=0}^{+\infty} \alpha_i \mathcal{E}\left([w(t)]^i\right), \tag{3}$$

where $\mathcal{E}(.)$ is the time average, i is the summation index, and the coefficients $\alpha_i \geq 0$ depend on the rectifier characteristics. Since the pulse has a repetition period of $T + T_{\mathrm{CP}}$, we can restrict the averaging on one period, giving

$$\mathcal{E}\left([w(t)]^i\right) = \frac{1}{T + T_{\mathrm{CP}}} \int_0^{T_{\mathrm{CP}}} [w(t)]^i \mathrm{d}t, \tag{4}$$

where the upper bound of the integral is set to T_{CP} since it is the maximal pulse duration. Since the modulated power signal is assumed to be band limited, the average of the real signal will be zero when i is odd (i.e., $\mathcal{E}\left([w(t)]^i\right) = 0$ when i is odd). On the other hand, the even order terms do not cancel. For instance, if we compute the second-order time average

$$\mathcal{E}\left([w(t)]^2\right) = \frac{1}{T + T_{\mathrm{CP}}} \frac{1}{4} \int_0^{T_{\mathrm{CP}}} \left[w_{\mathrm{P}}(t)e^{J\omega_{\mathrm{c}}t} + w_{\mathrm{P}}(t)^{*}e^{-J\omega_{\mathrm{c}}t}\right]^2 \mathrm{d}t. \tag{5}$$

When developing the square, two of the terms correspond to the Fourier transform of $w_{\mathrm{P}}(t)^2$ evaluated at $\pm 2\omega_{\mathrm{c}}$ and can be ignored given the low pass nature of $w_{\mathrm{P}}(t)$. Only the cross-terms remain, leading to

$$\mathcal{E}\left([w(t)]^2\right) = \frac{1}{T + T_{\mathrm{CP}}} \frac{1}{2} \int_0^{T_{\mathrm{CP}}} |w_{\mathrm{P}}(t)|^2 \mathrm{d}t. \tag{6}$$

Similarly, if we compute the fourth time average, the only remaining cross-term is

$$\mathcal{E}\left([w(t)]^4\right) = \frac{6}{T + T_{\mathrm{CP}}} \frac{1}{2^4} \int_0^{T_{\mathrm{CP}}} |w_{\mathrm{P}}(t)|^4 \mathrm{d}t. \tag{7}$$

We can generally induce that $\mathcal{E}\left([w(t)]^{2i}\right) \propto \int_0^{T_{\mathrm{CP}}} |w_{\mathrm{P}}(t)|^{2i} \mathrm{d}t$, and the output harvested current can be written as

$$i_{\text{out}} = \sum_{i=0}^{+\infty} \beta_i \int_0^{T_{\text{CP}}} |w_{\text{P}}(t)|^{2i} \mathrm{d}t = \sum_{i=0}^{+\infty} \beta_i \int_0^{T_{\text{CP}}} P(t)^i \mathrm{d}t, \tag{8}$$

where $P(t) = |w_{\text{P}}(t)|^2$ representing the power of the power pulse signal.

To simplify the optimization, we transform these expressions to a discrete time and replace the integrals by sums. The samples of $w_{\text{P}}(t)$ and $P(t)$ are denoted by $w_{\text{P}}[m]$ and $p[m]$, respectively.[1] The objective is to find the optimal values of $p[0], \ldots, p[L_{\text{cp}} - 1]$ that maximize the output harvested current subject to the average power constraint, the PAPR constraint (i.e., a peak constraint), and a positivity constraint. Thus, the optimization problem can be formulated as

$$\max_{p[0],\ldots,p[L_{\text{cp}}-1]} i_{\text{out}} \approx \sum_{i=0}^{+\infty} \beta_i \sum_{m=0}^{L_{\text{cp}}-1} p[m]^i, \tag{9}$$

subject to

$$\begin{aligned} &\frac{1}{L_{\text{cp}} + N} \sum_{m=0}^{L_{\text{cp}}-1} p[m] = P_{\text{av}}, \\ &p[m] \leq p_{\max}, \\ &p[m] \geq 0. \end{aligned} \tag{10}$$

The objective function is a polynomial function, which is convex given the positiveness of $p[0], \ldots, p[L_{\text{cp}} - 1]$. Moreover, the constraints correspond to a convex set of solution. The solution of the maximization of a convex function lies on the extreme of the feasible sets.

One possible solution for the above formalized problem which satisfies the Karush–Kuhn–Tucker (KKT) conditions is an almost rectangular pulse, where we can define

$$L = \left\lfloor \frac{(L_{\text{cp}} + N)P_{\text{av}}}{p_{\max}} \right\rfloor. \tag{11}$$

For the constraint to make sense and recalling that the power pulse samples has to be within the cyclic prefix, the average power is assumed to be smaller than the cyclic prefix multiplied by $p_{\max}$ ($P_{\text{av}} < L_{\text{cp}}\, p_{\max}$) and therefore the value of L is always less than the cyclic prefix $L < L_{\text{cp}}$. A solution is obtained by setting $p[m] = p_{\max}$ for $m = 0, \ldots, L - 1$ and the remaining power $p[L] = P_{\text{av}}(L_{\text{cp}} + N) - Lp_{\max}$.

Technically, implementing the last sample $p[L]$ is not really practical. From design point of view, it makes more sense to only consider the samples with full $p_{\max}$ amplitudes and discard the remaining one $p[L]$. Hence, we can safely assume that we want a signal that is purely rectangular within the cyclic prefix duration (Fig. 5).

Mathematically, one could argue that the nonzero samples with amplitude $p_{\max}$ could be spread within the cyclic prefix rather than creating a rectangular shape. However, from both implementation and interference point of view, it is better to

[1] Without loss of generality and for simplification, we consider that the bandwidth of the power pulse is approximately the same as the WIT system which is $\frac{N}{T}$ (i.e., band-limited). Hence, by Nyquist sampling theorem, there is no loss when sampling it in the time domain.

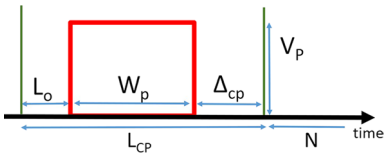

Fig. 5 Illustration of rectangular power signal parameters. Refer to Sect. 3.3 for the explicit definition of these parameters

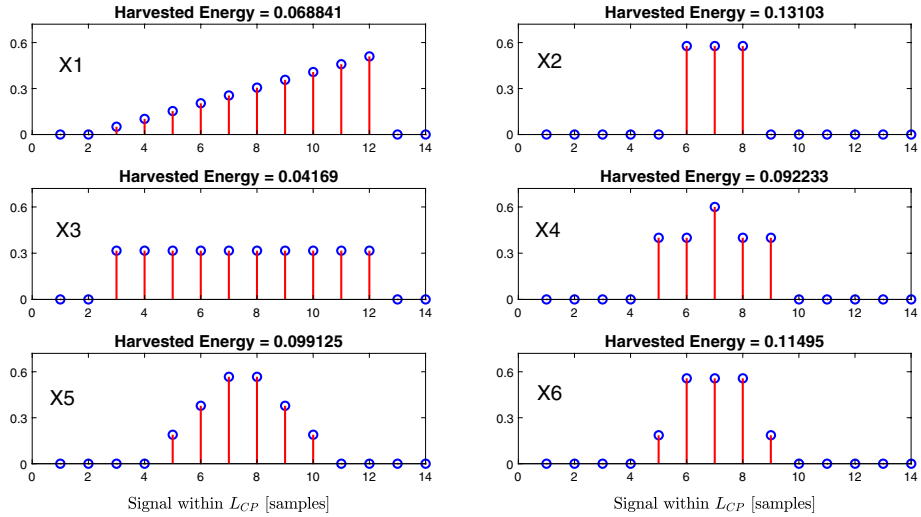

Fig. 6 Comparing different shapes of signals in terms of harvested energy using the nonlinear model of the rectifier

group these samples together in time as far as possible from the start of the following useful OFDM part rather than spreading them.

In order to compare the rectangular shape with other signal shapes, we provide an example illustrated in Fig. 6. In this example, we use the nonlinear model of the rectifier in equation 20 in [2] to compute the harvested energy for these various signal shapes. These signals are assumed to be within the cyclic prefix duration, and for the fairness of comparison, they all have equal average power. Besides, for this particular example, we assume that the PAPR constraint imposes that the instantaneous amplitude of any sample can not exceed 0.7. The results show that the rectangular shape signal X2 with the highest possible peak during the shortest possible duration provides the greatest amount of energy harvested.

In conclusion, the result of this optimization can be interpreted as having the smallest number of samples with the highest possible value instead of having a constant lower value all over the cyclic prefix. This concentration is better both in terms of harvested energy as well as from the point of view of interference. The model and parameters of this power signal are discussed in detail in the following subsection.

3.3 Power signal model and parameters

As mentioned above, a power signal is generated from a power head using a modulated rectangular pulse signal that is sent only during the cyclic prefix duration T_{cp}. Without loss of generality, we assume that the width and position of the rectangular pulse are set as

multiples of the sampling time ($T_s = \frac{T}{N}$) of the signal. Then, the baseband discrete-time signal representation of the power signal generated by the power head can be written as

$$w_P[m] = \begin{cases} V_p \text{ if } \left| m - \left(\frac{W_p}{2} + L_o \right) \right| \leq \frac{W_p}{2} \\ 0 \quad \text{otherwise,} \end{cases} \tag{12}$$

which is sent in a synchronized fashion during the duration $0 \leq m \leq N + L_{cp}$. The signal parameters are defined as follows and as shown in Fig. 5:

- L_o: represents the offset between the start of the cyclic prefix and the beginning of the rectangular pulse defined in terms of samples (the corresponding time is given by: $T_o = L_o\ T_s$).
- W_p: represents the width of the rectangular pulse defined in terms of samples (the corresponding time is given by: $T_w = W_p\ T_s$).
- V_p: represents the amplitude of the rectangular signal.

The discrete-time representation of the total transmitted power signal generated by the power head can be represented as:

$$x_P[m] = \sum_{b=-\infty}^{+\infty} w_P[m - b(N + L_{cp})], \tag{13}$$

where b is the index of the OFDM symbols transmitted. To avoid interference with the useful symbol duration, we restrict the rectangular pulse to be within the cyclic prefix duration such that $0 < L_o < L_{cp} - W_p$.

One important indicator is the distance between the end of the peak and the end of cyclic prefix duration L_{cp} that we refer to as "CP margin" and can be defined as

$$\Delta_{cp} = L_{cp} - (L_o + W_p). \tag{14}$$

The CP margin Δ_{cp} , which is defined in samples, indicates how much the pulse is near or far from the next useful OFDM symbol. In practice, Δ_{cp} should be positive otherwise the rectangular pulse overlaps with the useful OFDM symbol duration creating strong interference.

The choice of waveform parameters is influenced by some regulations and limitations. One of them is the limitation on PAPR where the regulation imposes that the peak power should not exceed 20 dB above the average power [40]. We can infer that the average transmitted power over one OFDM symbol can be expressed as:

$$P_{av} = \frac{P_P\ W_p}{N + L_{cp}}. \tag{15}$$

where the peak power is defined as $P_P = \frac{V_p^2}{R}$ and we assume that $R = 1$. Based on the maximal allowed PAPR, the minimal value of pulse width is set to

$$\frac{P_{peak}}{P_{av}} \leq \Upsilon_{max} \leftrightarrow W_p \geq W_{p,min} = \frac{N + L_{cp}}{\Upsilon_{max}}. \tag{16}$$

For example, if we consider the maximum PAPR $\Upsilon_{\max}$ to be 18 dB higher than the average power and we use the fact that the normal cyclic prefix in LTE standard is around 7% of the useful OFDM duration T. Then, the minimum width of the rectangular pulse will be $W_{\text{p,min}} = \frac{N+L_{\text{cp}}}{63} \approx \frac{1.07N}{63} \approx \frac{N}{58.87}$.

On the other hand, based on the current network setup, there might exist another limitation due to time travel difference between both transmitters. In many cases, the power head might be located closer to the IoT device than the base station. This is due to the difference in sensitivities of both systems, where energy harvesting requires higher power levels at the receiver. Due to the difference in travel time, the power signal could potentially arrive before the information signal which will create interference onto the previous useful OFDM symbol (see Fig. 4). So the rectangular peak offset L_{o} should be adjusted correctly to accommodate for such problem and should be greater than a minimum offset $L_{\text{o,min}}$.

4 Influence of power signal on information decoding chain

One important aspect of this work is to study the impact of the proposed power signal on the whole information transmission process. In this section, we highlight this effect by analyzing the influenced hardware components, signal processing operations, and data by conducting an interference analysis accompanied with interference evaluation and simulations.

4.1 Influenced data: interference analysis and simulations

4.1.1 Interference analysis

Even though we restrict the rectangular pulse to be within the cyclic prefix, interference on the useful OFDM symbol can still exist due to channel dispersion between the power head and the IoT device (see Fig. 4). This interference needs to be reduced as much as possible since high power levels are radiated by the power head that is located at a close distance from the IoT device. This is usually achievable since the cyclic prefix duration (L_{cp}) is normally chosen to be large enough to accommodate for information channel dispersion which is on the same order of magnitude, or higher than the (shorter) power channel dispersion. However, it still requires a careful setting of the parameters. The interference is derived based on the operations performed at the receiver. Then, the expressions are evaluated and the results are discussed in a practical scenario to illustrate the effect of the different parameters on this interference.

We assume a multipath wireless fading channel from both the power head and the base station towards the IoT device, and additive white Gaussian noise (AWGN) (see illustration in Fig. 7). The multipath channel can be modeled as a linear time-invariant filter. We directly consider the digital complex baseband equivalent channel impulse response taking into account the combination of transmit and receive filters as well as the physical channel, sampled at the sampling rate of the system $\frac{1}{T_{\text{s}}}$. The channel is assumed to be constant across the duration of an OFDM symbol.

In order to have a general analysis, we will consider the influence of U synchronized power heads instead of only one. This is due to the fact that power heads are typically

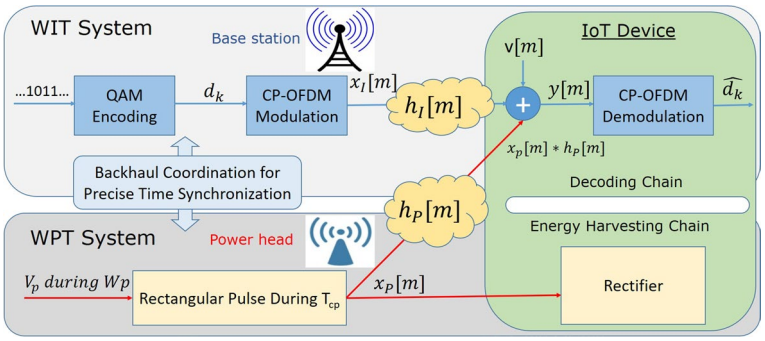

Fig. 7 Block Diagram representing the interference caused by the power signal $x_{\mathrm{p}}[m]$ due to the channel $h_{\mathrm{p}}[m]$ onto the information decoding chain at the IoT receiver

intensively deployed to provide sufficient power for energy harvesting. Accordingly, we denote by $h_{P_i}[m]$ the channel experienced by the power signal from the ith power head to the IoT device, and $h_I[m]$ represents the channel experienced by the information signal from the base station to the IoT device. All channels are assumed to have a maximum duration of L_{ch} taps.

The discrete time representation of the received signal at the input antenna of the CP-OFDM receiver can be expressed as follows:

$$y[m] = x_I[m] * h_I[m] + \underbrace{\sum_{i=1}^{U} x_P[m] * h_{P_i}[m]}_{\textbf{Interference}} + v[m], \tag{17}$$

where $x_I[m]$ is the OFDM information signal and $v[m]$ is the AWGN. Assuming perfect synchronization at the information receiver chain, the cyclic prefix part is discarded from the signal. Then, Fourier transform (FT) is applied to the received windowed signal. The nth OFDM demodulated symbol on the kth subcarrier of the receiver can be expressed as:

$$\hat{d}_k[n] = d_k[n] + \sum_{i=1}^{U} \Gamma_{k,i}[n] + \tilde{v}[n], \tag{18}$$

where $\tilde{v}[n]$ is the filtered Gaussian noise, $d_k[n]$ is the recovered symbol, and $\Gamma_{k,i}[n]$ is the interference caused by the rectangular pulse of the ith power head filtered by its respective channel $h_{P_i}[m]$ onto the kth subcarrier of the nth CP-OFDM symbol. Since the interference analysis is performed during one CP-OFDM symbol duration ($N + L_{\mathrm{cp}}$), the index n can be dropped. Considering the effect of the ith power head, the interference on the kth information subcarrier in the digital domain can be written as:

$$\Gamma_{k,i} = \frac{V_{\mathrm{p}}}{\sqrt{N}} \sum_{m=L_{\mathrm{cp}}}^{N} \sum_{l=1}^{L_{ch}} h_{P_i}[l]\ \mathrm{rect}\left[\frac{m - l - \frac{W_{\mathrm{p}}}{2} - L_{\mathrm{o}}}{W_{\mathrm{p}}}\right] e^{-J\frac{2\pi km}{N}}, \tag{19}$$

Table 1 Parameters used in simulation

CP-OFDM parameters	
Carrier frequency	2 GHz
Sampling frequency	2 MHz
Sub-carrier spacing Δ_f	3.90625 kHz
Number of subcarriers N	512
Sampling period Ts	0.5 µs
Useful symbol duration N (T)	512 samples (256 µs)
Cyclic prefix duration L_{cp} (T_{cp})	36 samples (18 µs)
Channel indoor parameters	
Average delay spread DS	38 ns
Delay scaling parameter r_τ	3
Noise	− 120 dBm

where

$$\text{rect}\left[\frac{m-\alpha}{\beta}\right] = \begin{cases} 1 \text{ if } |m-\alpha| \leq \frac{\beta}{2} \\ 0 \text{ otherwise.} \end{cases}$$

Then, the total interference on the kth information subcarrier coming from all power heads can be written as:

$$\Gamma_k = \sum_{i=1}^{U} \Gamma_{k,i}. \tag{20}$$

4.1.2 Interference evaluation using simulations

To evaluate the expression of interference above, we consider an indoor scenario with only one power head located 2 m ($d_{P_i} = 2\,\text{m}$) from an IoT device. This distance is intentionally chosen to be small so that the transmitted power remains relevant for energy harvesting at the IoT device. In addition, this can be viewed as a worst case scenario in terms of the interference this power signal can create on the information transfer. To complete the setup, the base station is located 15 m away ($d_I = 15\,\text{m}$) from the IoT device. The respective free space path-loss values are $PL_I = 61.9842$ dB for the information signal and $PL_P = 44.483$ dB for the power signal. This setup is illustrated in Fig. 3. The average transmitted power from the power head is fixed to be $P_{P,Tx} = 23$ dBm while the average transmitted power from the base station is considered to be $P_{I,Tx} = 10$ dBm. We define the power gap Δ_{P} (in dB scale) to be difference in power levels between WIT and WPT such that:

$$\Delta_{\text{P}} = (P_{P,Tx} - PL_P) - (P_{I,Tx} - PL_I). \tag{21}$$

The parameters of the OFDM transmission used in this simulation are provided in Table 1. It is important to note that the cyclic prefix size is based on the delay spread of the channel between the information transmitter and the receiver (i.e., information channel) while the delay spread highlighted in the above table corresponds to the channel between the power transmitter and the receiver (i.e., power channel).

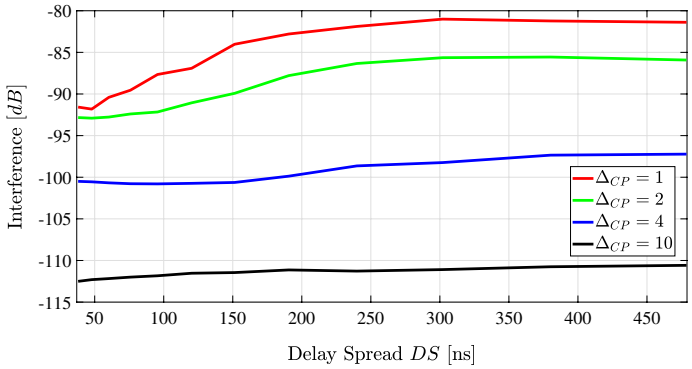

Fig. 8 Interference versus delay spread for different values of $\Delta_{cp} = \{1, 2, 4, \text{and } 12\}$

On the other hand, the amount of interference expressed in (19) is highly influenced by the delay spread (DS) of the power channel. Therefore, we evaluated the interference as a function of the delay spread for different Δ_{cp} values. The results are illustrated in Fig. 8. It is noticed the interference for a particular Δ_{cp} are almost the same, regardless of the delay spread value. This means that the behavior of the interference for a given Δ_{cp} is maintained regardless of the delay spread value chosen. Therefore, for the rest of this simulation section, we will use the value of the delay spread defined in Table 1. This value and other channel parameters defined in Table 1 are based on an "Indoor office" model extracted from the WINNER II Channel Models [41]. The delay scaling parameter r_τ controls the rate of decay of the power delay profile. Based on these, the power delay profile has been randomly generated and associated with the channel between the power head and the IoT device. This profile is kept constant for all simulations presented below where each simulation is based on 2000 independent channel realizations generated from this power delay profile. The channel impulse response takes into account the transmit and receive filters in addition to the physical channel.

Fixing the pulse offset to L_o and the pulse width to W_p, the total interference onto every subcarrier is computed. The results are shown in Fig. 9 for 4 different sets of parameters. We notice that the interference values can vary across subcarriers with various patterns depending on the parameters. In order to be able to compare more easily the effects of the different parameters, the interference in Fig. 9 is then further averaged over the subcarriers to obtain Fig. 10.

To highlight the importance of the CP margin Δ_{cp} on the interference, we first fix the pulse offset to $L_o = 6$ samples and vary the rectangular pulse width W_p to evaluate the average interference caused by this power head onto the useful OFDM symbol. This average interference is represented in Fig. 10 as a function of the CP margin Δ_{cp}, which directly varies with the width W_p. As expected, this figure shows that interference increases when the CP margin Δ_{cp} decreases. In other words, the farther the pulse is from the edge of the cyclic prefix, the lower the interference is (except obviously when Δ_{cp} becomes negative). On the other hand, the interference is then evaluated with a fixed pulse width $W_p = 20$ samples and a varying pulse offset L_o. The results are also shown in Fig. 10 as a function of the CP margin Δ_{cp}, which also directly varies with the pulse offset L_o. Both curves exhibit very similar behavior with a slight difference which is related to the change in the pulse height V_p while

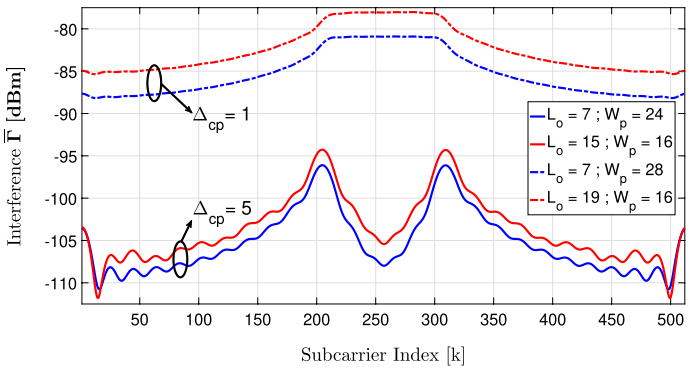

Fig. 9 Interference per subcarrier averaged over 2000 channel realizations when $\Delta_{cp} = 5$ for ($L_o = 7$, $W_p = 24$) and ($L_o = 15, W_p = 16$); and when $\Delta_{cp} = 1$for ($L_o = 7, W_p = 28$) and ($L_o = 19, W_p = 16$)

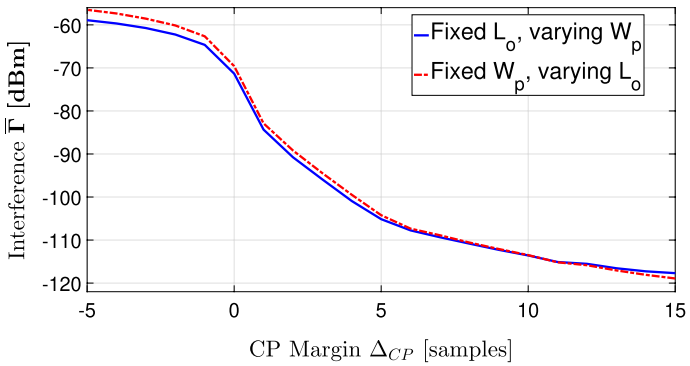

Fig. 10 Average interference as function of Δ_{cp}. The continuous line corresponds to $L_o = 6$ samples and varying W_p while the dotted line corresponds to $W_p = 20$ samples and varying L_o

varying W_p to maintain a fixed average power. This identical behavior proves that the CP margin is the main parameter affecting the interference. In particular, the changes to the peak voltage (that are related to the pulse width W_p to maintain a fixed average power) are negligible with respect to variations of the CP margin Δ_{cp}. Hence, regardless of whether the width or the offset is varying, we can approximate the interference as a direct function of the CP margin Δ_{cp}. To further confirm the result, one can look again at Fig. 9 which plots the per-subcarrier interference for four sets of parameters where each couple of parameters corresponds to the same CP margin Δ_{cp}. Once again, the curves exhibit very similar behaviors with small differences due to the reasons discussed above.

In order to evaluate the potential performance loss of the information transmission, we computed the SINR (signal-to-interference and noise-ratio) at the IoT device for the considered setup, based on the powers transmitted by the different nodes, and taking into account the path losses. The SINR is illustrated in Fig. 11 as a function of the CP margin Δ_{cp}. As expected, increasing the cyclic prefix margin Δ_{cp} is beneficial for the performance of the information transmission. It can also be observed that, with the proposed setup, low interference levels (SINR $>$ 20 dB) can easily be obtained with a margin of $\Delta_{CP} = 5$ samples, for instance with $L_o = 6$, which provides

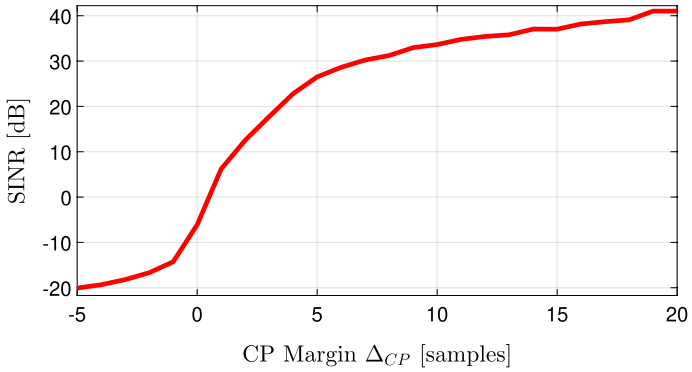

Fig. 11 SINR of the information signal for different values of Δ_{cp}

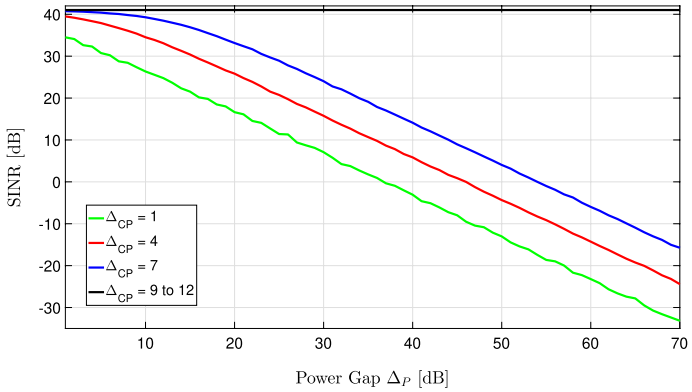

Fig. 12 SINR for the information signal of different Δ_P values while fixing Δ_{CP} from 1 $\rightarrow$ 12

a good protection against synchronization errors, and with $W_p = 24$ which is already much higher than the minimum value ($W_{p,min} = 9$ for this setup) related to the peak power regulations. This leads to a negligible interference even in the scenario considered here, where the power head is very close to the IoT device. It is important to be reminded that the number of samples, defined for signal parameters, depends on the system setup and the chosen sampling rate of the system and it is assumed that both WIT and WPT share the same sampling rate and are synchronized.

In the same simulation setup, we consider another case where we fix the cyclic prefix margin and vary the power gap Δ_P. The SINR as function of Δ_P is plotted in Fig. 12 for different values of Δ_{CP}. The result shows that as Δ_P increases, SINR decreases until it becomes flat at $\Delta_{CP} > 8$. The degradation in SINR is due to the effect of small channel taps that are magnified as Δ_P increases. The flattening shows that regardless of how big the power gap is the performance of the information transmission is not affected as long as the rectangular pulse is at a safe distance away from the useful part of the OFDM symbol. Hence, Δ_{CP} should be greater than 8 samples in this particular simulation setup and particular parameter values.

It is important to note that farther power heads (or longer paths) have longer delay which could potentially spread outside the cyclic prefix duration (L_{cp}). These can also belong to different cells where we have lack of synchronization between the information

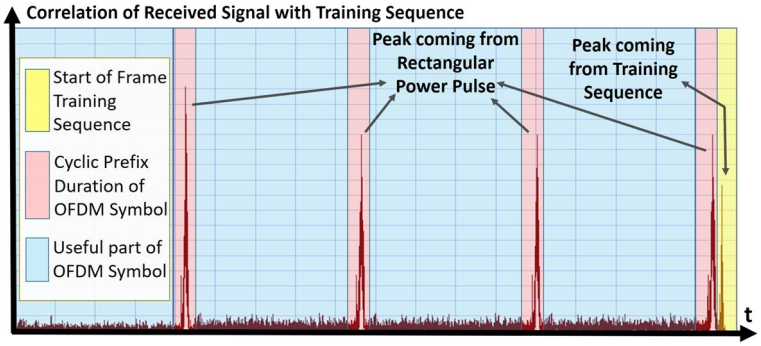

Fig. 13 The figure shows an example of flipping and correlating four received CP-OFDM symbols with a certain training sequence. This simple synchronization method can provide errors since the starting of the frame is not going to be detected properly (i.e., synchronization error)

and power transmitters. However, they have much smaller power level. One potential solution is: by assuming that the value of the rectangular pulse can be known at the receiver (i.e., deterministic), hence they could be canceled out using estimation techniques. Moreover, they do not incur a high risk of ADC saturation. We do not explicitly take these cases into consideration here. This is left for future work.

4.2 Influenced signal processing operations

Several signal processing operations might be influenced by the power signal and synchronization is one of them. High power levels of the power signal might influence/deteriorate the synchronization operation. For instance, if only a simple correlation based synchronization method is utilized, the rectangular pulse can sometimes provide higher peaks than those of the training sequences as shown in Fig. 13. There are many ways to overcome this issue by using more robust synchronization methods. In the setup here, we use "self-reference" frame synchronization method that can be derived from least squares expression of the Moose algorithm [42]. This frame detection method is expressed as:

$$\hat{i} = \arg\max \frac{\sum_{L}^{N_t-1} y[n+i+N_t]y^*[n+i]}{\sqrt{\sum_{L}^{N_t-1} |y[n+i]|^2}\sqrt{\sum_{L}^{N_t-1} |y[n+i+N_t]|^2}} \tag{22}$$

where $y[n]$ is the received signal, N_t is the size of the training sequence (considered periodic), L is the number of channel taps, and $\hat{i}$ is the starting frame index. The advantage of this method is that it removes the effect of the rectangular power pulse by dividing the correlation by the received signal power as shown in the denominator of the above Eq. (22). Besides, high power peaks can be advantageous and can have a positive contribution in enhancing the synchronization process of the wireless information transfer especially that both the rectangular pulse parameters and training sequence can be known at the receiver. However, we are not going to detail this possibility in this paper and can be left for future research.

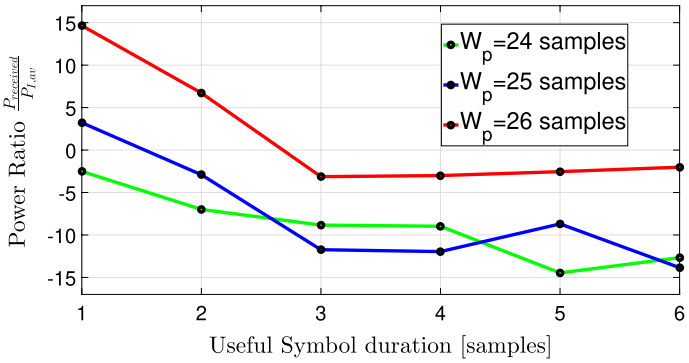

Fig. 14 Investigation of possible ADC saturation for the first few samples of the three smallest Δ_{CP}, i.e., $W_p = \{24, 25, 26\}$ and $L_o = 6$ with acceptable SINR, i.e., $\Delta_{CP} \geq 4$ at SINR $\geq$ 15 dB

4.3 Influenced components

High power levels of the power heads during the cyclic prefix (L_{cp}) could saturate the ADC of the information decoding chain at the IoT device, especially given that the difference in sensitivities of both systems (WPT and WIT) can reach up to 30 or 40 dB in some cases. In our proposed waveform design, the power signal is transmitted only during the cyclic prefix duration L_{cp}. Therefore, the automatic gain controller (AGC) can be designed to ignore the power received during the cyclic prefix (L_{cp}). In that case, the saturation is not problematic as the samples are discarded anyway. However, in the case of channel dispersion, the first samples of the useful OFDM part become at risk of ADC saturation when the power difference (Δ_P) between WIT and WPT is high and the rectangular pulse is spread in time due to channel dispersion. Using the same setup, consider the cases of cyclic prefix margin where SINR is acceptable (i.e., $\Delta_{CP} \geq 4$ at $SINR \geq 15$ dB). Knowing that ADC saturation is highly probable when the cyclic prefix margin is the smallest possible, we consider the three smallest possible Δ_{CP} as a worst case scenarios and observe the power gap at first few samples of the useful part of OFDM symbol. The results in Fig. 14, shows a maximum ≤ 15 dB power gap which proves that there is no risk of ADC saturation on the first samples in an SINR acceptable region.

5 Measurements

In this section, we are going to focus on the measurements that are done for the communication part while the energy harvesting measurements were presented in section V of our work in [39]. These measurements show that, given the same amount of energy, it is better to focus energy in high peaks rather than spreading it. Specifically, the results show that the proposed rectangular waveform with narrow width can improve the DC voltage at the receiver (i.e., improves the energy harvesting performance). In this work, we conduct real measurements to investigate the performance of the information transmission in the presence of this power signal and compare the results with the simulated ones. In this experiment, we utilize the following hardware components:

- Two Software Defined Radio Re-configurable Devices NI USRP-2944R: Each USRP (universal software radio peripheral) is made up of two daughter boards. One USRP is used as a transmitter with one daughter board allocated to the base station and the other one for the power head. The second USRP uses one of its daughter boards for the IoT receiver device.
- Three identical omnidirectional antennas: one for each node.
- A workstation with LabVIEW software.
- A switch device (PCI Express CPS-8910): to use 2 USRPs on one workstation.
- Chassis Remote Control Cable: to connect the workstation with the switch, and the switch with the USRPs.

The setup of the measurements is illustrated in Fig. 15. The software consists of a classical OFDM transmission scheme synchronized with a rectangular pulse signal that is sent during the cyclic prefix duration. The experiment is carried out inside a laboratory illustrating an indoor channel scenario where the transmitters and the receiver are placed 3 m apart for case I and 4 m apart for case II. The main parameters used are summarized in Table 2. The parameters are chosen to match the capability of the utilized hardware. The remaining main parameters that we vary depending on the measurement case are as follows: the rectangular width W_{p}, the rectangular offset L_{o}, cyclic prefix margin Δ_{CP}, and the power gap Δ_{P} which is defined above as the difference in transmitted power levels between the power head and the base station. Unlike in the simulation case, the power gap is not affected by the path-loss because both transmitters have the same distance away from the IoT receiver ($d_{\mathrm{p}} = d_i = 4$). However, the gap is affected by the gain allocated to each daughter board (i.e., each transmitter) which can be adjusted differently ($G_{P,Tx} \neq G_{I,Tx}$) where $G_{P,Tx}$ represents the gain of the transmitted power signal and $G_{I,Tx}$ represents the gain of transmitted information signal. Besides, the ratio of power levels of both transmitted signals, denoted by A_r, can also affect the power gap such that $A_r = 20 \log \frac{V_p}{V_i}$ where V_i is the amplitude of the information signal. Hence, in this measurement, the power gap can be expressed as:

$$\Delta_{\mathrm{P}} = G_{P,Tx} - G_{I,Tx} + A_r. \tag{23}$$

The average SINR is also used as a performance metric for the OFDM transmission. The value of average SINR is obtained by averaging over 2000 channel realizations as well as averaging across the subcarriers.

In the first case, we consider fixing the power gap of the transmitters (i.e., fixing Δ_{P}) and varying the cyclic prefix margin Δ_{CP} by either varying the offset L_{o} or the width W_{p}. We also considered either fixing the average peak power P_{peak} or by fixing the average power P_{av} of the transmitted power signal. The results of these measurements are plotted on Fig. 16. The blue line corresponds to fixing $L_{\mathrm{o}} = 6$ samples and varying W_{p} with fixed peak power P_{peak}, the black line corresponds to fixing $W_{\mathrm{p}} = 20$ samples and varying L_{o} with also with fixed peak power P_{peak}, the red line corresponds to fixing $L_{\mathrm{o}} = 6$ samples and varying W_{p} with fixed average power P_{av}, and the green line corresponds to fixing $W_{\mathrm{p}} = 20$ samples and varying L_{o} with also fixed average power P_{av}. The following points can be induced from the results:

Table 2 Measurement parameters of WIT

Power signal parameters used at transmitter	
Carrier frequency	2 GHz
Sampling frequency	2 MHz
Sampling period *Ts*	0.5 µs
Cyclic prefix size L_{cp}	36 samples
Gain of power signal $G_{P,Tx}$	0 : 31.5 dB
Rectangular offset L_o (when fixed)	6 samples
Rectangular width W_p (when fixed)	20 samples
Amplitude V_p	10 x V_i
Ratio of amplitude *Ar*	20.73 dB
Information signal parameters used at transmitter and receiver	
Carrier frequency	2 GHz
Actual sampling rate	20 MHz
Oversampling factor	10
Sampling frequency	2 MHz
Bandwidth	1.980 MHz
Intermediate frequency	6 MHz
Modulation	QPSK
Sub-carrier spacing Δ_f	3.90625 kHz
Number of subcarriers *N*	512
Number of inactive subcarriers	5
Sampling period *Ts*	0.5 µs
Useful symbol duration *N* (*T*)	512 samples (256 µs)
Cyclic prefix duration L_{cp} (T_{cp})	36 samples (18 µs)
Training sequence type	IEEE 802.11a short
Training sequence size	160 samples
Pulse shape parameters	Raised Cosine
Information signal parameters used at transmitter only	
Gain of information signal $G_{I,Tx}$	6 dB
Number of bits transmitted	1024
Information signal parameters used at receiver only	
Case I distance *d*	3 m
Case II distance *d*	4 m
Synchronization method	OFDM synchronization
Symbol timing recovery method	Max energy
Frame detection method	Self reference w/power norm.

1 The behavior of all results look almost identical. This means that, for a fixed power gap, the key parameter is the cyclic prefix margin Δ_{CP}, which can be changed by either varying the offset L_o or the width W_p. This observation is in line with the results derived in the previous simulation section.
2 The shape of the curves is similar to the ones in the simulation section, specifically in Fig. 11.
3 The average SINR value for $\Delta_{CP} \geq 5$ is flat around 20 dB, which is a SINR reference value indicating almost no interference coming from the power signal onto the useful part of OFDM symbol. We call this the "safe" region.
4 In the region where $3 \leq \Delta_{CP} \leq 5$, the average SINR has slightly decreased with respect to the SINR reference value which indicates a slight degradation of perfor-

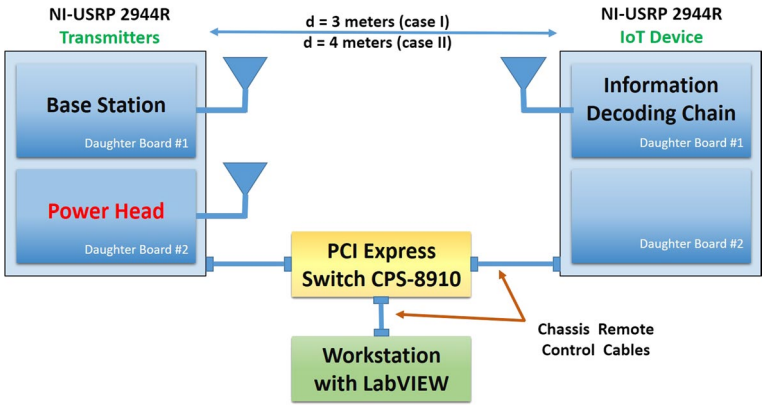

Fig. 15 Block diagram that illustrates the measurement setup

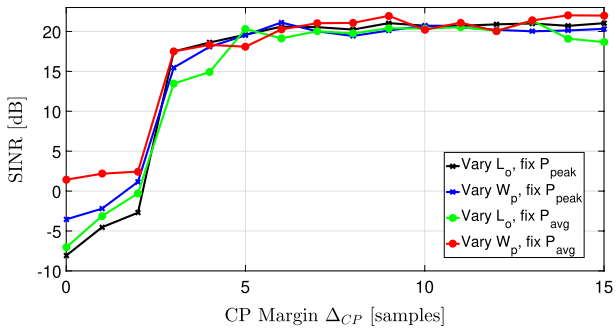

Fig. 16 Case I: Fixing power gap $\Delta_p = 30$ dB and varying Δ_{CP} by either varying L_o or W_p and by either fixing the average peak power P_{peak} or by fixing the average power P_{av}

mance. This means that there is a small amount of interference coming from the power signal. We call this region the "boundary" region.

5 It is noticeable that the average SINR has sharply decreased with respect to the reference value (20 dB) when $\Delta_{CP} < 3$ indicating a huge degradation of performance. This is due to the effect of the large channel taps which results in huge interference. We call this region the "interference" region.

6 It is important to note also that the decreasing slope of the SINR depends on channel taps. In other words, the power delay profile used in the simulations are not the same as the one obtained from the real measurements. This explains the discrepancy between the slope in Fig. 16, which is sharp, and the slope in Fig. 11. The delay spread of the channel affects the boundary of the three regions named above: interference, boundary, and safe regions.

In the second case, we vary the power gap Δ_P and fix the cyclic prefix margin Δ_{CP} with $L_o = 6$ and $W_p = 20$. We consider different values of Δ_{CP} in each region discussed above: interference $\Delta_{CP} = \{1, 2\}$, boundary $\Delta_{CP} = \{3, 4, 5\}$, and safe $\Delta_{CP} = \{10, 12\}$ regions. The results are plotted in Figs. 17 and 18 and the following can be concluded:

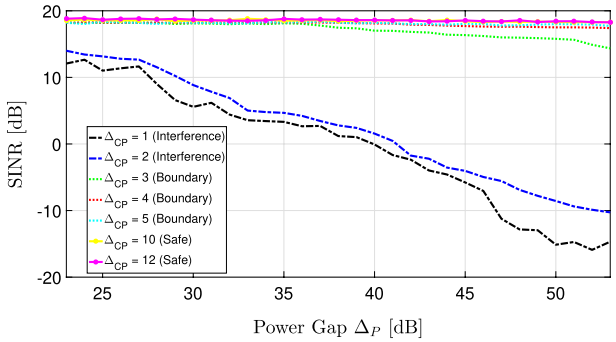

Fig. 17 Case II: Fixing the cyclic prefix margin Δ_{CP} to $\{1, 2, 3, 4, 5, 10, 12\}$ and varying the power gap Δ_p. We consider Δ_{CP} values from the: interference, boundary, and safe regions

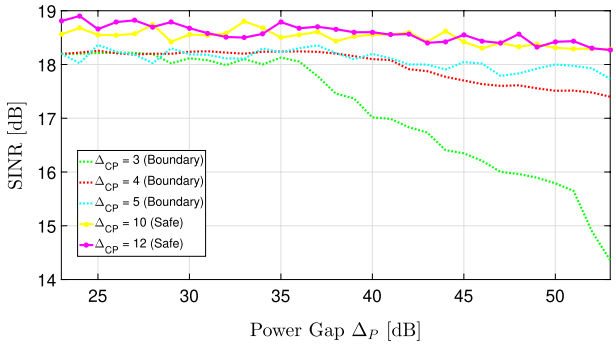

Fig. 18 This plot also represents Case II, i.e., fixing Δ_{CP} and varying Δ_p, but for only the boundary and safe regions, i.e., $\Delta_{CP} = \{3, 4, 5, 10, 12\}$. Zooming in to see their behavior

1 In the interference region (i.e., when $\Delta_{CP} = \{1, 2\}$), it is obvious from Fig. 17 that the average SINR decreases as the power gap Δ_P increases. This is expected because higher power is given to the rectangular pulse and accordingly to the interference it creates.
2 In the boundary region (i.e., when $\Delta_{CP} = \{3, 4, 5\}$), we notice from Fig. 18 that there is a slight decrease in the average SINR. This is explained by the fact that the lower parts of the impulse response, that can usually be ignored, start to have an impact at higher power gap Δ_P, as shown in Fig. 18. This issue has been highlighted at the end of Sect. 4.1.2 when talking about farther power heads.
3 In the safe region (i.e., $\Delta_{CP} = \{10, 12\}$), we notice from Figs. 17 and 18 that the average SINR is not affected and it is flat for all power gap Δ_P measured.

Hence, it is induced that choosing the "safe" Δ_{CP} value can help avoiding interference onto the useful part of the OFDM symbol (i.e., not affecting WIT performance) even when there is a 53 dB power gap between the information and the power transmitters. This is in line with the simulation results illustrated in Fig. 12.

6 Conclusion

This work is a continuation of our proposed waveform in [39] that presents a novel technique which allows WIT and WPT to coexist with essentially no degradation of their respective performance as long as a good time synchronization is kept. The proposed waveform is a modulated rectangular pulse that is sent during the cyclic prefix of the CP-OFDM information system. Given a limited amount of transmitted power, the interference evaluation using simulations, energy harvesting measurements in [39], and communication performance measurements show that a short pulse with a safe Δ_{CP} value and sufficient offset L_o (to counter any delay difference or synchronization issues) provide good energy harvesting performance as well as significantly reduce the amount of interference caused by the power signal onto the information signal. This work studies also the practical implication of the power signal onto the information decoding chain at the receiver. In the future, one may investigate the effect of farther power heads, that are already synchronized with the base station, using stochastic geometric techniques. On the other hand, the receiver architecture can be further studied taking into consideration this proposed waveform. Especially that the pulse itself may even help in the synchronization of the different devices of the system. The results are promising especially as they have been validated through practical measurements using hardware devices.

Abbreviations

SWIPT	Simultaneous Wireless Information and Power Transfer
WPT	Wireless Power Transfer
WIT	Wireless Information Transfer
PAPR	Peak to Average Power Ratio
CP-OFDM	Cyclic Prefix Orthogonal Frequency-Division Multiplexing
IoT	Internet of Things
RFID	Radio Frequency Identification
M2M	Machine-to-Machine
MIMO	Multiple-Input Multiple-Output
NN	Neural Network
RF	Radio Frequency
DC	Direct Current
ADC	Analog to Digital Converter
PSK	Phase Shift Keying
CSI	Channel State Information
TS	Time Switching
PS	Power Splitting
RC	Resistor Capacitor
FT	Fourier Transform
KKT	Karush–Kuhn–Tucker
CP	Cyclic Prefix
SINR	Signal-to-Interference and Noise-Ratio
AGC	Automatic Gain Controller
NI-USRP	National Instruments Universal Software Radio Peripheral
PCI	Peripheral Component Interconnect

Acknowledgements

The authors are grateful to Ivan Stupia and Nafiseh Janatian for their assistance during NI-USRP measurements.

Author contributions

HK and JL came up with idea and conceived the study. HK wrote the manuscript and conducted the simulations and measurements. JL had a general advising role. FR had an external advisory role and contributed to the theoretical formulation of the problem. TF and CW helped in developing the software of the measurements. All authors participated in the discussions and provided essential contributions to the research. All authors read and approved the final manuscript.

Funding

This work is supported by Université catholique de Louvain under the ARC SWIPT Project. Part of this work was published in [39] and presented at the 2019 IEEE International Conference on Communications (ICC) in Shanghai, China.

Availability of data and materials

Data sharing is not applicable to this article.

Declarations

Competing interests
The authors declare that they have no competing interests.

Received: 5 July 2021 Accepted: 25 July 2022
Published online: 03 September 2022

References

1. Y. Zeng, B. Clerckx, R. Zhang, Communications and signals design for wireless power transmission. IEEE Trans. Commun. **65**(5), 2264–2290 (2017)
2. B. Clerckx, E. Bayguzina, Waveform design for wireless power transfer. IEEE Trans. Signal Process. **64**(23), 6313–6328 (2016)
3. L.R. Varshney, Transporting information and energy simultaneously, in *Proceedings of the International Symposium on Information Theory* (2008), pp. 1612–1616
4. H. Ju, R. Zhang, Throughput maximization in wireless powered communication networks. IEEE Trans. Wirel. Commun. **13**(1), 418–428 (2014)
5. B. Clerckx, Z. Bayani Zawawi, K. Huang, Wirelessly powered backscatter communications: waveform design and SNR-energy tradeoff. IEEE Commun. Lett. **21**(10), 2234–2237 (2017)
6. H. Lee et al., Resource allocation techniques for wireless powered communication networks with energy storage constraint. IEEE Trans. Wirel. Commun. **15**(4), 2619–2628 (2016)
7. R. Zhang, C.K. Ho, MIMO broadcasting for simultaneous wireless information and power transfer. IEEE Trans. Wirel. Commun. **12**(5), 1989–2001 (2013)
8. H. Son, B. Clerckx, Joint beamforming design for multi-user wireless information and power transfer. IEEE Trans. Wirel. Commun. **13**(11), 6397–6409 (2014)
9. J. Xu, L. Liu, R. Zhang, Multiuser MISO beamforming for simultaneous wireless information and power transfer. IEEE Trans. Signal Process. **62**(18), 4798–4810 (2014)
10. J. Park, B. Clerckx, Joint wireless information and energy transfer in a two-user MIMO interference channel. IEEE Trans. Wirel. Commun. **12**(8), 4210–4221 (2013)
11. J. Park, B. Clerckx, Joint wireless information and energy transfer in a k-user MIMO interference channel. IEEE Trans. Wirel. Commun. **13**(10), 5781–5796 (2014)
12. J. Park, B. Clerckx, Joint wireless information and energy transfer with reduced feedback in MIMO interference channels. IEEE J. Sel. Areas Commun. **33**(8), 1563–1577 (2015)
13. A.A. Nasir, X. Zhou, S. Durrani, R.A. Kennedy, Relaying protocols for wireless energy harvesting and information processing. IEEE Trans. Wirel. Commun. **12**(7), 3622–3636 (2013)
14. Y. Huang, B. Clerckx, Joint wireless information and power transfer for an autonomous multiple-antenna relay system. IEEE Commun. Lett. **19**(7), 1113–1116 (2015)
15. Y. Huang, B. Clerckx, Relaying strategies for wireless-powered MIMO relay networks. IEEE Trans. Wirel. Commun. **15**(9), 6033–6047 (2016)
16. K. Huang, E.G. Larsson, Simultaneous information and power transfer for broadband wireless systems. IEEE Trans. Signal Process. **61**(23), 5972–5986 (2013)
17. X. Zhou, R. Zhang, C.K. Ho, Wireless information and power transfer in multiuser OFDM systems. IEEE Trans. Wirel. Commun. **13**(4), 2282–2294 (2014)
18. D.W.K. Ng, E.S. Lo, R. Schober, Wireless information and power transfer: energy efficiency optimization in OFDMA systems. IEEE Trans. Wirel. Commun. **12**(12), 6352–6370 (2013)
19. X. Zhou, R. Zhang, C.K. Ho, Wireless information and power transfer: architecture design and rate-energy tradeoff. IEEE Trans. Commun. **61**(11), 4754–4767 (2013)
20. K. Huang, E.G. Larsson, Simultaneous information and power transfer for broadband wireless systems. IEEE Trans. Signal Process. **61**(23), 5972–5986 (2013)
21. M. Varasteh, B. Rassouli, B. Clerckx, Wireless information and power transfer over an AWGN channel: nonlinearity and asymmetric Gaussian signaling, in *Proceedings of the IEEE Information* (2017). arXiv:1705.06350
22. M. Varasteh, E. Piovano, B. Clerckx, A learning approach to wireless information and power transfer signal and system design, in *IEEE International Conference on Acoustics, Speech and Signal Processing (ICASSP)* (2019), pp. 4534–4538
23. J. Kim, B. Clerckx, P.D. Mitcheson, Prototyping and experimentation of a closed-loop wireless power transmission with channel acquisition and waveform optimization, in *Proceedings of the IEEE Wireless Power Transfer Conference (WPTC)* (2017)
24. J. Kim, B. Clerckx , P.D. Mitcheson, Experimental analysis of harvested energy and throughput trade-off in a realistic SWIPT system, in *2019 IEEE Wireless Power Transfer Conference (WPTC), London, UK* (2019), pp. 1–5
25. T. Perera, D. Jayakody, S. Sharma, S. Chatzinotas, J. Li, Simultaneous wireless information and power transfer (SWIPT): recent advances and future challenges. IEEE Commun. Surv. Tutor. **20**(1), 264–302 (2017)
26. B. Clerckx, R. Zhang, R. Schober, D.W.K. Ng, D.I. Kim, H.V. Poor, Fundamentals of wireless information and power transfer: from RF energy harvester models to signal and system designs. IEEE J. Sel. Areas Commun. **37**(2), 1–30 (2019)
27. K. Huang, C. Zhong, G. Zhu, Some new research trends in wirelessly powered communications. IEEE Wirel. Commun. **23**(2), 19–27 (2016)
28. X. Lu, P. Wang, D. Niyato, D.I. Kim, Z. Han, Wireless networks with RF energy harvesting: a contemporary survey. IEEE Commun. Surv. Tutor. **17**(2), 757–789 (2015)
29. N. Pan, M. Rajabi, N.B. Carvalho, Bandwidth analysis of RF-DC converters under multisine excitation. IEEE Trans. Microw. Theory Technol. **66**(2), 791–802 (2018)

30. C.R. Valenta, M.M. Morys, G.D. Durgin, Theoretical energy-conversion efficiency for energy-harvesting circuits under power optimized waveform excitation. IEEE Trans. Microw. Theory Technol. **63**(5), 1758–1767 (2015)
31. A. Collado, A. Georgiadis, Optimal waveforms for efficient wireless power transmission. IEEE Microw. Wirel. Compon. Lett. **24**(5), 354–356 (2014)
32. D.I. Kim, J.H. Moon, J.J. Park, New SWIPT using PAPR: how it works. IEEE Wirel. Commun. Lett. **5**(6), 672–675 (2016)
33. M. Maso, S. Lakshminarayana, T.Q.S. Quek, H.V. Poor, A composite approach to self-sustainable transmissions: rethinking OFDM. IEEE Trans. Commun. **62**(11), 3904–3917 (2014)
34. B. Li, W. Xu, S. Li , J. Lin, Energy efficient power allocation in OFDM-based CRNs with cyclic prefix power transfer, in *2015 IEEE 81st Vehicular Technology Conference (VTC Spring), Glasgow, UK* (2015), pp. 1–5
35. R.F. Buckley , R.W. Heath, Selective OFDM transmission for simultaneous wireless information and power transfer, in*2019 IEEE Global Communications Conference (GLOBECOM), Waikoloa, HI, USA* (2019), pp. 1–6
36. H. Kassab, J. Louveaux, Gabor expansion for simultaneous wireless power and information transfer (SWIPT): interference analysis, in *Proceedings of the 39th Symposium on Information Theory and Signal Proceedings in Benelux* (2018), pp. 847–862
37. B. Clerckx, Wireless information and power transfer: nonlinearity, waveform design, and rate-energy tradeoff. IEEE Trans. Signal Process. **66**(4), 847–862 (2018)
38. I. Krikidis, S. Timotheou, S. Nikolaou, G. Zheng, D.W.K. Ng, R. Schober, Simultaneous wireless information and power transfer in modern communication systems. IEEE Commun. Mag. **52**(11), 104–110 (2014)
39. H. Kassab, J. Louveaux, Simultaneous wireless information and power transfer using rectangular pulse and CP-OFDM, in *2019 IEEE International Conference on Communications (ICC)*, Shanghai, China (2019), pp. 1–6
40. Rules and regulations of Federal Communication Commission (FCC), codified in Title 47 of the Code of Federal Regulations (CFR), Part 15
41. P. Kyosti et al., Part 1: Channel Models, WINNER II Project D1.1.2 V1.1, version 1.1 (2007)
42. P. Moose, A technique for orthogonal frequency division multiplexing frequency offset correction. IEEE Trans. Commun. **42**(10), 2908–2914 (1994)

Publisher's Note